MCD spectroscopy of hexanuclear Mn(III) salicylaldoxime single-molecule magnets

Justin M. Bradley,*[a] Andrew J. Thomson,[a] Ross Inglis,[b] Constantinos J. Milios,[b,c] Euan K. Brechin[b] and Stergios Piligkos[d]

Received 10th June 2010, Accepted 23rd July 2010
DOI: 10.1039/c0dt00634c

The hexanuclear cages $[Mn_6O_2(R\text{-sao})_6L_2(EtOH)_x(H_2O)_y]$ "Mn_6" behave as single-molecule magnets (SMMs) below a characteristic blocking temperature. As with $[Mn_{12}O_{12}(O_2CR)_{16}(H_2O)_4]$ "Mn_{12}" the electronic absorption spectra are rather featureless, yielding little information on the electronic structure of the magnetic ions. Low temperature Magnetic Circular Dichroism (MCD) spectra afford greater resolution of the optical transitions and also probe the magnetic properties of the system. Both the ground state spin and blocking temperature of the Mn_6 cages are determined by subtle structural perturbations of a generic Mn_6O_2 core. Absorbance and MCD spectra are reported for $[Mn_6O_2(Et\text{-sao})_6\{O_2CPh(Me)_2\}_2(EtOH)_6]$ (**1**), $[Mn_6O_2(Et\text{-sao})_6\{O_2CPh\}_2(EtOH)_4(H_2O)_2]$ (**2**), $[Mn_6O_2(sao)_6\{O_2CPh\}_2(EtOH)_4]\cdot EtOH$ (**3**) and the trinuclear precursor $[Mn_3O(Et\text{-sao})_3(MeOH)_3](ClO_4)$ (**4**) cast into polymer film. SMM behaviour has previously been observed using magnetic susceptibility measurements on powder and single-crystal samples. The ligand field environment of the magnetic ions is assumed to be similar in (**1**) and (**2**) and their different blocking temperatures are attributed to the magnitude of the effective exchange constant. The MCD spectra of (**1**) and (**2**), in which the ground state spin $S = 12$, show that the ligand field environments of the Mn ions are almost identical and that magnetic hysteresis persists for isolated molecules when crystal packing forces are removed. The subtle structural differences between (**1**) and (**2**) are manifested in the field dependence of the MCD response at different wavelengths that reflect changes in band polarisation. The MCD spectrum of (**3**) contains features not apparent in those of (**1**) and (**2**). These are attributed to 5-coordinate Mn(III), which is unique to (**3**) among the compounds studied. (**3**) has ground state spin $S = 4$, a lower blocking temperature and consequently no observable hysteresis in the MCD down to 1.7 K. Comparison of the MCD spectra of (**1**)–(**3**) to that of (**4**) confirms the integrity of the Mn_6O_2 core when these materials are cast into polymer film.

Introduction

The characteristic feature of single-molecule magnets (SMMs) is the very slow relaxation of the magnetic moment following exposure to a magnetic field. This offers the possibility of the storage of information at the molecular scale of density. The behaviour arises from the combination of a large ground state electron spin S and a *negative* uniaxial magnetic anisotropy D. This leads to a barrier to the re-orientation of the molecular magnetic moment. Below a characteristic temperature called the blocking temperature the relaxation of the magnetic moment following the application of a magnetic field becomes extremely slow.[1,2] The discovery[3,4] that the mixed valence $Mn(III)_8Mn(IV)_4$ cluster $[Mn_{12}O_{12}(O_2CR)_{16}(H_2O)_4]$, "$Mn_{12}$" exhibits magnetic properties characteristic of SMMs has led to increasing interest in high nuclearity Mn(III) complexes in recent years.[5,6] The d^3 Mn(IV) ions in Mn_{12} contribute little to the magnetic anisotropy of the cluster whereas the static Jahn–Teller distortion of the d^4 Mn(III) ions provides the anisotropy needed. The serendipitous self assembly or directed synthesis of Mn(III) containing clusters[7–9] has therefore been a rich field in the search for new SMMs with higher blocking temperatures than Mn_{12}. Whilst this has led to the discovery of many new SMMs[5,10–20] it is only recently that the blocking temperature of Mn_{12} has been surpassed. An alternative strategy is the targeted distortion of a generic Mn_6 core in order to maximise the anisotropy barrier[21–27] which is proportional to the product DS^2.

The family of hexanuclear cages has the general formula $[Mn_6O_2(R\text{-sao})_6L_2(EtOH)_x(H_2O)_y]$ where R-saoH$_2$ is a derivatised salicylaldoxime, R = H or CH_3CH_2 and L is a carboxylate which acts as a ligand to one or more of the Mn ions. The cage contains only Mn(III) ions with elongated bonds along one axis due to a static Jahn–Teller distortion of the d^4 electronic configuration. The structure consists of two approximately co-planar, stacked, offset $[Mn_3\text{–}\mu_3\text{-}O^{2-}]^{7+}$ triangular motifs, each Mn ion within the triangular unit having a crystallographic equivalent in the other Mn_3O triangle. For R = H the bridging phenolic oximes are almost planar leading to dominant antiferromagnetic exchange within triangular moieties (Fig. 1). Each Mn ion has at least one elongated Mn–O contact which defines the local z axis (easy axis

[a]*School of Chemistry, University of East Anglia, Norwich, UK NR4 7TJ. E-mail: justin.bradley@uea.ac.uk; Tel: +44 (0)1603 593051*
[b]*School of Chemistry, The University of Edinburgh, Joseph Black Building, West Mains Road, Edinburgh, Scotland EH9 3JJ*
[c]*Current address: Department of Chemistry, University of Crete, 71003, Herakleion, Greece*
[d]*Department of Chemistry, University of Copenhagen, Universitetsparken 5, 2100, Copenhagen, Denmark*

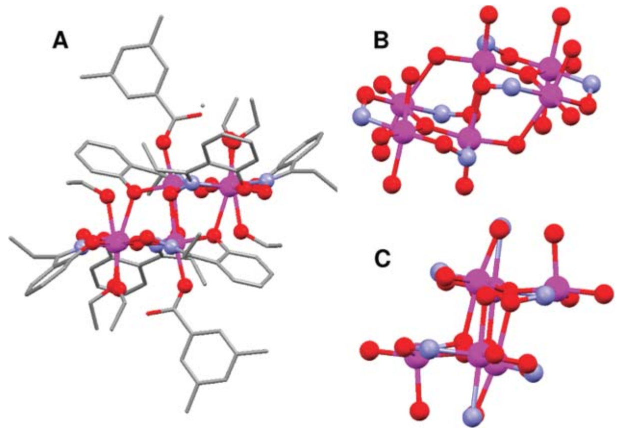

Fig. 1 (A) The structure of (1) illustrating the generic $Mn_6O_2(R\text{-sao})_6L_2(EtOH)_x(H_2O)_y$ cage structure, (B) the core of (1) in which all Mn(III) ions are six-coordinate, (C) the core of (3) in which the increased inter-planar Mn–O distance leads to five-coordinate Mn(III) ions at the extrema of the cage. Magenta = Mn, red = O, blue = N, the carbon backbone is de-emphasised for clarity.

of magnetisation). Three short bonds to nitrogen and oxygen donors from the sao^{2-} ligands and a further bond to the μ-bridging oxide of the core define a hard plane perpendicular to this. Two of the manganese ions are six-coordinate with a distorted octahedral geometry. In one of these the coordination sphere is completed by a carboxylate oxygen and a long (*ca.* 2.4 Å) contact to an oxygen from a sao^{2-} ligand of the other triangular subunit. The other six-coordinate ion has long contacts to water and/or solvent molecules. The third inequivalent Mn ion is five-coordinate with distorted square pyramidal geometry, the oxygen from the corresponding sao^{2-} ligand in the opposite triangular subunit being too distant (at approximately 3.3 Å) to form a covalent bond.

Increasing the bulk of R causes distortion of the bridging phenolic oxime, described by a torsion angle ϕ in the Mn–O–N–Mn linkage. Substitution with R = CH_3CH_2 is sufficient to induce a change in the dominant exchange within each triangular moiety from antiferromagnetic to ferromagnetic.[23,25] A further consequence of the twisting induced when R = CH_3CH_2 is to decrease the longest inter-planar Mn–O distance to around 2.4 Å such that all the Mn ions are six-coordinate with distorted octahedral geometry, the coordination of the remaining two Mn ions being essentially unaltered from R = H, as illustrated in Fig. 1. Despite the different connectivity between the triangular subunits for R = H and CH_3CH_2 the dominant exchange between triangles remains ferromagnetic in each case, resulting in ground state spin $S = 4$ for R = H and 12 for R = CH_3CH_2.[25]

Here we present the absorbance and magnetic circular dichroism (MCD) spectra of three members of this family of cages, $[Mn_6O_2(Et\text{-sao})_6\{O_2CPh(Me)_2\}_2(EtOH)_6]$ (**1**), $[Mn_6O_2(Et\text{-sao})_6\{O_2CPh\}_2(EtOH)_4(H2O)_2]$ (**2**), and $[Mn_6O_2(sao)_6\{O_2CPh\}_2(EtOH)_4]\cdot EtOH$ (**3**), in addition to the precursor $[Mn_3]$ cluster $[Mn_3O(Et\text{-sao})_3(MeOH)_3](ClO_4)$ (**4**). Both (**1**) and (**2**) have theoretical anisotropy barriers of 62 cm^{-1} (89 K) surpassing that of Mn_{12}. However, the smaller average value of ϕ in (**2**) than in (**1**) results in weaker ferromagnetic exchange, $J = +0.9$ cm^{-1} in (**2**) compared to +1.6 cm^{-1} in (**1**). As a consequence the energy separation of the spin excited states in (**2**) is small, the $S = 11$ first excited state being only 5 cm^{-1} above the ground state, and the total spin S is a poor quantum number. Therefore the effective barrier to relaxation of the magnetisation, U_{eff}, in (**2**) is considerably lower than the theoretical maximum value at only 36.8 cm^{-1} compared to around 60 cm^{-1} in (**1**) and slow relaxing forms of Mn_{12}.[28]

Whilst (**3**) and (**4**) are also known to be SMMs, their ground state spins are $S = 4$ and 6, giving rise to anisotropy barriers $U_{eff} = 19.5$ and 39.0 cm^{-1} respectively.[29,30] However, the reported U_{eff} of (**4**) is greater than the theoretical maximum value calculated from the product DS^2 since magnetisation reversal in this case is hindered by weak intermolecular coupling. Removal of the intermolecular coupling by casting into polymer film lowers the effective barrier to ≤ 27.6 cm^{-1}.[29] Thus, samples of (**3**) and (**4**) cast into PMMA film are expected to have blocking temperatures of approximately 1 K, too low for MCD detected hysteresis to be evident at 1.7 K.

Crystal structures are available for all of the series. Slow relaxation of the magnetisation has been demonstrated in powder and single-crystal samples. In the case of (1) the AC susceptibility shows a peak in the out-of-phase component of the magnetisation, which can be diagnostic of SMM behaviour, at temperatures up to 7 K. However, structural modifications which influence the magnetic properties are subtle and may be influenced by crystal packing interactions in addition to the steric requirements of side chain modifications. Since practical applications such as data storage at a molecular level necessarily require that the molecules be well isolated from one another it is desirable to study the magnetic properties of molecules dispersed within an inert matrix. It has been demonstrated for Mn_{12} that dispersion within a polymer film produces samples suitable for study by MCD.[31] This approach is particularly suited to the study of SMMs as it provides a simultaneous probe of ligand field environment of the chromophores and magnetic properties of the molecule as a whole[32,33] in samples which are robust and re-usable.

Experimental

Preparation of PMMA films

The clusters **1**–**4** were synthesised according to previously published procedures.[27,29,30] All further materials were used as received without further purification. Approximately 2 mg of **1**–**3** were dissolved in 500 μl of $CHCl_3$. **4** is only sparingly soluble in $CHCl_3$. 2 mg of sample was therefore pre-dissolved in a minimum amount of 2-propanol prior to mixing with sufficient $CHCl_3$ to make the final volume up to 500 μl. The resulting solutions of **1**–**4** were then each mixed with 200 mg of polymethylmethacrylate (PMMA) dissolved in 1 ml of $CHCl_3$ before dropping on to a Petri dish. The solution was covered with another Petri dish and allowed to evaporate overnight resulting in a film of **1**–**4** contained in a PMMA matrix. Films were prized free with a razor blade, softening with warm water for a few seconds if necessary.

MCD of PMMA films

All spectra were recorded on a Jasco J-810 spectropolarimeter. Samples were placed in an Oxford Instruments SM4 split coil superconducting solenoid capable of providing magnetic fields of up to 5 T. A variable temperature insert allows the sample temperature to be maintained at 1.7–200 K. Films were checked to ensure that they did not cause depolarisation of the beam by monitoring their effect on the circular dichroism (CD) spectrum of a nickel tartrate standard. MCD spectra were recorded over the wavelength range 850–250 nm. In the range 850–480 nm the monochromater slits were fixed at a separation of 120 μm. The separation of the slits was allowed to vary automatically to maintain a fixed bandwidth of 2 nm in a second scan over the wavelength range 520–250 nm.

Spectra were recorded at 4.2 K and 5 T for the purpose of assignment and normalisation. The measured optical elipticity was converted to an approximate difference in extinction coefficient for left and right circularly polarised light ($\Delta\varepsilon$) by comparison of the room temperature absorbance to solution samples of known concentration. The estimated product c.l for the films can then be substituted into the Beer–Lambert law. Hysteresis measurements were performed by measuring spectra at 1.7 K at discrete fields in the cycle 0 - +5 - −5 - +5 T.

Results and discussion

Assignment of MCD spectra

The room temperature absorbance and 4.2 K, 5 T MCD spectra of **1**–**4** are shown in Fig. 2. The spectra are scaled so as to compensate for the different number of Mn(III) chromophores between (**1**)–(**3**) and (**4**). (**1**) was additionally shown to have no further MCD intensity in the energy range 5000–12 000 cm^{-1} (data not shown). The spectra of (**1**) and (**2**) are almost indistinguishable from one another. Further, despite each molecule containing three

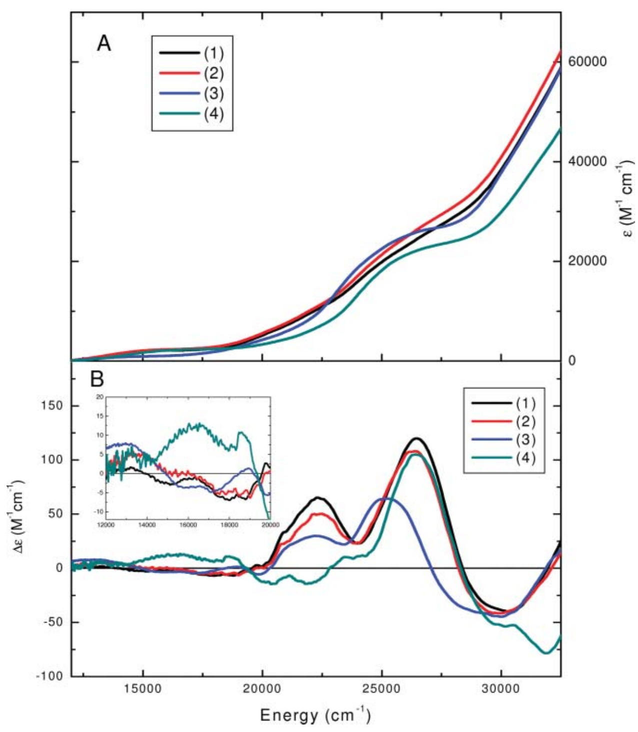

Fig. 2 Room temperature absorbance (panel A) and 4.2 K 5 T MCD (panel B) of (**1**)–(**4**). Spectra of (**4**) are normalised to account for the number of chromophores per molecule. The inset of panel B shows the region between 12 000 and 20 000 cm^{-1} on an expanded scale.

Table 1 Peak positions of Gaussians fitted to the 4.2 K 5 T MCD of $Mn_{12}C_{15}$ and (**1**)–(**4**). The transition marked * is assumed due to 5-coordinate manganese, that marked # is approximately 5% the intensity of the corresponding transition in (**1**)–(**3**)

Compound	Energy ($\times 10^3$ cm^{-1})							
$Mn_{12}C_{15}$	13.5	15.5	—	18.0	19.6	21.2	23.5	26.0
(**1**)	13.0	15.0	—	18.2	20.9	22.3	24.0	26.4
(**2**)	13.4	—	—	18.4	20.8	22.2	22.9	26.5
(**3**)	12.9	15.8	17.3*	19.2	20.7	21.4	22.4	25.4
(**4**)	16.5	—	—	18.9	20.1	22.1	23.4#	26.6

crystallographically inequivalent Mn(III) ions, the features in the low temperature MCD spectra of (**1**) and (**2**) can be rationalised in terms of single ion transitions of a d^4 electronic configuration. Any small shifts in the energies of the d–d and charge transfer transitions in (**1**) and (**2**) due to differences in the coordination environments of the inequivalent ions are therefore unresolved. The crystal structure of (**1**) and (**2**) shows that the local symmetry of the Mn(III) ions is lower than C_2. In such low symmetry ligand fields the degeneracy of the d-orbitals is lifted completely. As a result the high spin d^4 configuration gives rise to four spin-allowed transitions rather than the single ^5E to $^5T_2$ transition predicted for true octahedral symmetry. For moderate strength octahedral ligand fields, a spin forbidden ^5E to $^3T_1$ transition is predicted to occur at similar energy to the spin-allowed transition. This corresponds to a change in configuration from $t_{2g}{}^3e$ to $t_{2g}{}^4$ and gives rise to up to three transitions in lower symmetry ligand fields. Thus for the Mn(III) ions in (**1**) and (**2**) a maximum of seven d–d transitions are predicted at energies below where charge transfer transitions would be expected to arise. Table 1 lists the peak positions obtained from the 4.2 K, 5 T MCD spectra of (**1**) and (**2**) by Gaussian deconvolution. All compounds also have MCD peaks of greater intensity at energies of 30 000 cm^{-1} and above which are assumed to be charge transfer transitions, possibly between the sao π orbitals and Mn(III). These data are not analysed here since the absorbance of the PMMA film is such that the magnitude of the observed optical rotation is unreliable. The observed energies of the absorption bands, though not their relative intensities, are similar to those previously reported for Mn_{12} in which the MCD intensity was thought to arise mainly from the Mn(III) ions. The different distribution of band intensities between Mn_{12} and (**1**) and (**2**) are unsurprising given the different coordination environment and intricacies of magnetic exchange pathway between the two classes of compounds. The lowest energy spin-allowed transition corresponds to shifting electron density from the d_{z^2} to the $d_{x^2-y^2}$ orbital and is therefore an approximate measure of the magnitude of the Jahn–Teller distortion which is mainly responsible for the inequivalence of the local *z*-axis and *xy* plane.[34] Since it is this distortion that gives rise to the SMM behaviour it is desirable that this be as large as possible and the energy of this $^5B_1$ to $^5A_1$ transition is comparable in (**1**) and (**2**) to that of $Mn_{12}Ac$ (see Table 1) and much greater than that in Mn(III) containing minerals.

The MCD spectrum of (**3**) contains additional features which are attributed to the 5-coordinate Mn ions at the exterior of the Mn_6 core. These ions are in a distorted square based pyramidal coordination environment which would be expected to give rise to a similar ordering in energy of electronic configurations but with different splittings between ground and excited states to a distorted octahedral geometry with a unique easy axis. Therefore, four of the six Mn ions in (**3**) are expected to give rise to bands similar to those in (**1**) and (**2**) whilst two give rise to distinct features in the MCD. Indeed the well resolved, intense bands at around 22 000 and 26 500 cm^{-1} have only approximately 60% of the intensity of the corresponding bands in (**1**) and (**2**). Hence, by virtue of the accompanying change in ligation of two of the chromophores, the nature of the intra-subunit exchange coupling is immediately apparent from the band pattern and intensity in the low temperature MCD spectrum.

The spectrum of (**4**) is distinct from all other members of the series, lacking the large positive feature at 22 000 cm^{-1} and having a broad positive band at around 16 500 cm^{-1} rather than two negative bands, suggesting that the magnetic core of (**1**)–(**3**) is not cleaved by the film casting process. The band at approximately 26 500 cm^{-1} is similar in intensity to the corresponding bands in (**1**) and (**2**), which also contain only 6-coordinate Mn and have dominant ferromagnetic intra-subunit magnetic exchange. The intensity of this band therefore appears to be diagnostic of Mn coordination and hence the sign of the magnetic exchange despite the drastic change in ligation between (**4**) and the other members of the series. The triangular $[Mn_3–\mu_3\text{-}0^{2-}]^{7+}$ motif in (**4**) is capped by a perchlorate ion, an extremely weak ligand, which provides an oxygen atom to each of the Mn ions. The cages (**1**)–(**3**) contain no capping perchlorate groups and so differences in the MCD spectra of (**1**)–(**3**) and (**4**) do not definitively preclude cleavage of the Mn_6O_2 core into two Mn_3O triangles. However, since the dominant exchange interaction in (**4**) is ferromagnetic and the clusters have similar uniaxial zero field splittings, cleavage of (**1**) and (**2**) to give analogues of (**4**) with $S = 6$ would be expected to result in similar magnetic properties. Hysteresis measurements at 1.7 K clearly show this not to be the case.

Hysteresis at 1.7 K

Fig. 3 and 4 show hysteresis measurements at 1.7 K for the series (**1**)–(**4**) at energies of approximately 22 000 cm^{-1} and 26 500 cm^{-1} corresponding to identical transitions in the different cages according to the assignments outlined in the previous section. The MCD of (**1**) and (**2**) show hysteresis effects at this temperature although the hysteresis loops of both are 'pinched' significantly. All transitions in (**1**) and (**2**) have a similar pinching of the hysteresis around zero field. Although the hysteresis effects are small they are undoubtedly real, as demonstrated by the lack of any such effects for (**3**) and (**4**) when measured under equivalent conditions. The observed hysteresis in (**1**) and (**2**) are remarkably similar to each other and distinct from Mn_{12} despite the U_{eff} of (**1**) being almost double that of (**2**) and similar to those of the Mn_{12} family. Since (**1**) and (**2**) exhibit such similar hysteresis behaviour despite the blocking temperature of (**1**) being significantly higher than that of (**2**) it seems unlikely that cooling below 1.7 K would result in an increase in either the apparent coercive field or remnant magnetisation. Indeed the rate of relaxation of the magnetisation in (**1**) has been shown to be independent of temperature below 2.0 K. It seems likely that the difference in behaviour between Mn_6 and Mn_{12} in MCD detected hysteresis measurements arises from relaxation of the structure upon casting into polymer film. The MCD detected hysteresis loops of (**1**) and (**2**) are strikingly similar to those

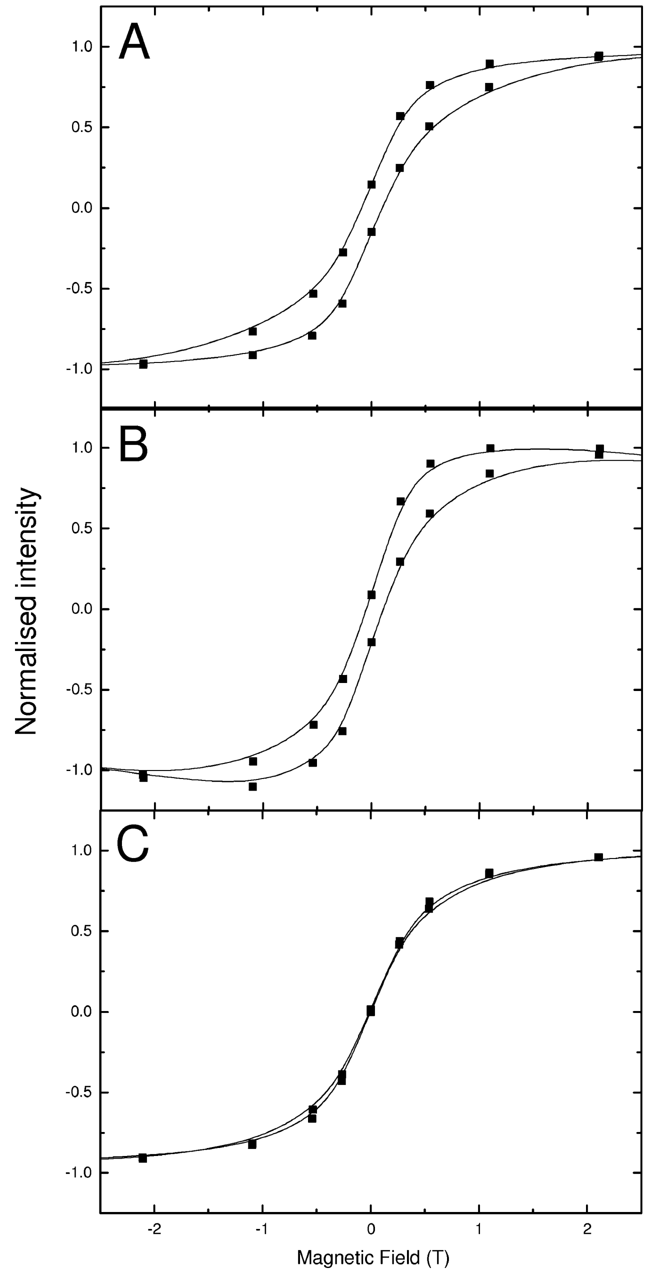

Fig. 3 Hysteresis measurements for (**1**) at 22 300 cm^{-1} (panel A), (**2**) at 21 600 cm^{-1} (panel B) and (**3**) at 22 500 cm^{-1} (panel C). The MCD spectrum of (**4**) has no intensity at similar energy.

detected using SQUID magnetometry on single-crystal samples exposed to large hydrostatic pressures.[35,36] High pressure X-ray crystallography showed that this loss of coercivity is due to flattening of the Mn–O–N–Mn torsion angles weakening the pairwise ferromagnetic exchange between metal centres, and that this effect is greatest for the metal ions which lie at the periphery of the cluster. An applied pressure of 1.5 GPa lowers two of the three torsion angles by around 5 degrees, fits of the magnetisation data show that this leaves the cluster anisotropy D almost unaffected but leads to a change in spin ground state and increased 'nesting' of the spin excited states resulting in the anisotropy barrier being lowered to around 50% of the value at ambient pressure. The pairwise ferromagnetic exchange

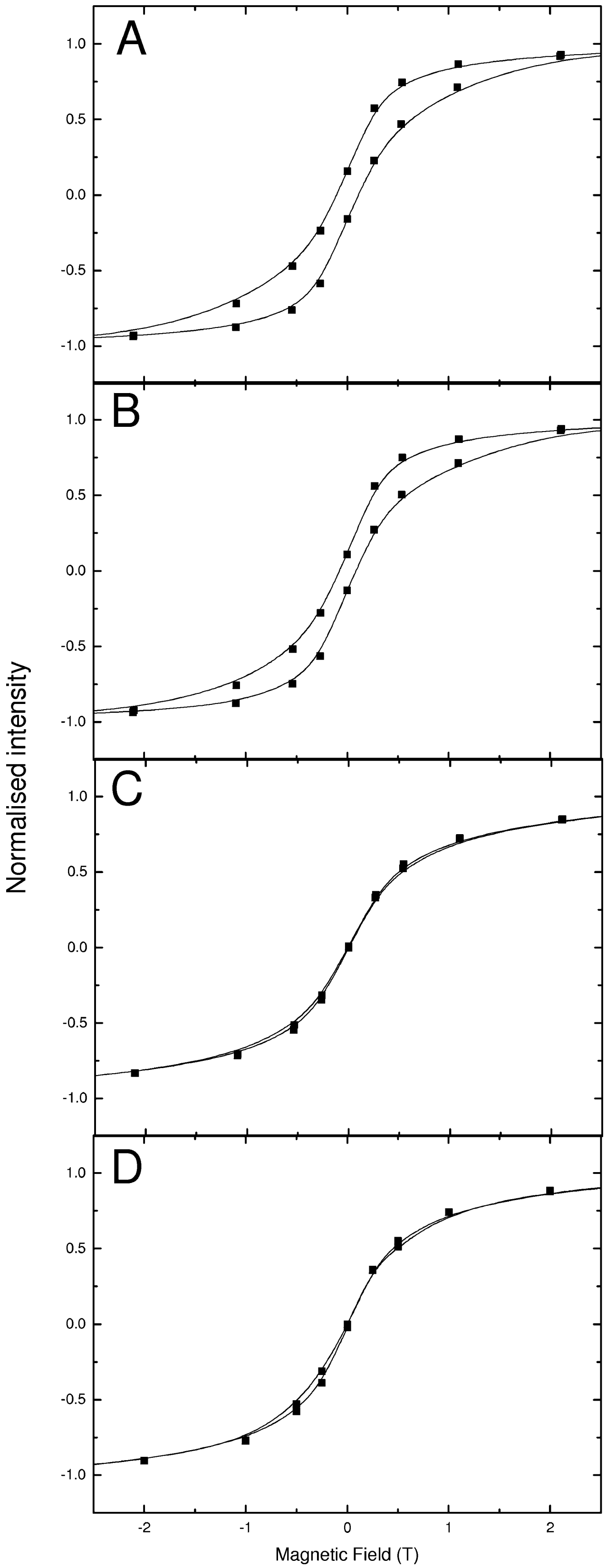

Fig. 4 Hysteresis measurements for (**1**) at 26 400 cm^{-1} (panel A), (**2**) at 26 500 cm^{-1} (panel B), (**3**) at 25 300 cm^{-1} (panel C) and (**4**) at 26 600 cm^{-1} (panel D).

between Mn(III) centres in Mn_{12} is not dependent on distortion of the bridging carboxylate ligands and the exchange parameters show little dependence on pressure. Rather the effect of pressure on Mn_{12} is to induce interconversion between slow and fast relaxing Jahn–Teller isomers.[37–40] The better agreement between susceptibility (solid state) and MCD (solution or polymer film) detected hysteresis in Mn_{12} is presumably therefore due to the greater rigidity of the cage.

An alternative explanation for the observed difference in behaviour of Mn_{12} and Mn_6 is the change in mechanism of relaxation of the magnetisation. In the Mn_6 cages the dominant mechanism of relaxation is *via* S-mixing[41,42] due to the relatively weak ferromagnetic exchange. In the Mn_{12} series the dominant mechanism is quantum tunnelling through the anisotropy barrier.[1,43–45] Indeed, magnetisation measurements on oriented single crystals of (**1**) show tunnelling transitions between spin states to be induced by small transverse (perpendicular to the molecular z-axis) fields. For a randomly (or close to randomly) oriented 'powder' sample in the MCD experiment, the vast majority of the ensemble will experience some transverse component of the magnetic field. This will induce spin relaxation at different applied fields for each orientation within the powder average, smearing out the peaks in relaxation rate observed for single-crystal samples.

All bands in the spectra of (**1**) and (**2**) retain between 5 and 20% of their 5 T intensity upon removal of the magnetic field and have coercive fields of approximately 1000G. There is however no consistent pattern for which bands retain the greatest percentage of their 5 T intensity at zero field between (**1**) and (**2**). In SMMs, only magnetisation along the molecular z-axis is retained upon removal of the magnetic field. Thus, in the MCD of SMMs, the degree of retention of intensity upon removal of the magnetic field is indicative of the amount of xy polarisation of the band. Since the molecular z-axis is the easy axis of magnetisation, bands which saturate more easily are also predicted to retain the greatest proportion of their 5 T intensity upon removal of the magnetic field. Hysteresis and magnetisation measurements at 1.7 K therefore indicate that bands of similar energies which presumably arise due to identical one-electron excitations on the Mn chromophores have slightly different polarisation ratios between (**1**) and (**2**). Given the similarity of the other parameters describing the magnetic properties of the core, this may be due to the differences in the distribution of the angles between the local and molecular z-axes in (**1**) and (**2**). Whilst the excitation of the electron is, to a first approximation, localised on a single ion, the band polarisation is expressed in coordinates which diagonalise the spin of the system, that is the molecular axes. Table 2 lists the angles formed between the elongated axes of the Mn(III) ions (the local z-axes) and those perpendicular to the plane containing the three ions (the molecular z-axis). Despite the probable relaxation of the structure as determined by X-ray crystallography upon casting the samples into PMMA film the variation in these angles between

Table 2 Calculated angles θ in degrees between the local Jahn–Teller axes of the Mn ions and the molecular z-axis for (**1**) and (**2**)

Compound	θ_1	θ_2	θ_3	θ_{av}	σ_θ
(**1**)	10.88	11.42	12.17	11.49	0.65
(**2**)	9.54	12.58	12.92	11.68	1.86

(**1**) and (**2**) remains a possible explanation for the differences in observed band polarisation.

Relaxation of remnant magnetisation at 1.7 K

Both (**1**) and (**2**) retain a small percentage of their 5 T MCD intensity on removal of the magnetic field provided the sample temperature remains below 2 K. This is consistent with the onset of temperature independent SMM behaviour observed by AC susceptibility. However, the intensity of this residual MCD decays over a period of minutes (see Fig. 5), in contrast to the relaxation time predicted from susceptibility measurements which is of the order of months at $T < 2$ K. The residual MCD of both compounds does not decay to zero. Fitting of the decay indicates small but finite intensity for several bands as $t \rightarrow \infty$ (see Table 3). The phenomenon of slow relaxation of the magnetisation is not restricted to zero field measurements. The intensity of the MCD response at 1.7 K is almost independent of field for applied fields greater than 2 T (see Fig. 3). However for lower applied fields small changes in $\Delta\varepsilon$ are observed for ~10^2 s after stepping the field (see Fig. 5) despite both the Hall voltage (which monitors the static field at the sample) and cernox resistance (which monitors sample temperature) remaining constant during this time period. Such effects are not observed in the 1.7 K MCD of (**3**) suggesting this phenomenon is a consequence of SMM behaviour. Within error the time constant for the decay of the magnetisation of (**1**) at small applied fields is identical to the slow phase of the biexponential decay observed at zero field. The decay of the zero field magnetisation of (**2**) is best fitted to a single exponential which is intermediate between the fast and slow phases of (**1**). It is unclear whether the biexponential decay observed for (**1**) at zero field is due to the overlap of bands with different relaxation characteristics or represents true biphasic behaviour of a single band. However, it has not proved possible to deconvolute wavelength scans collected at zero field after magnetising the sample into fast and slow relaxing components based on the peak positions listed in Table 1.

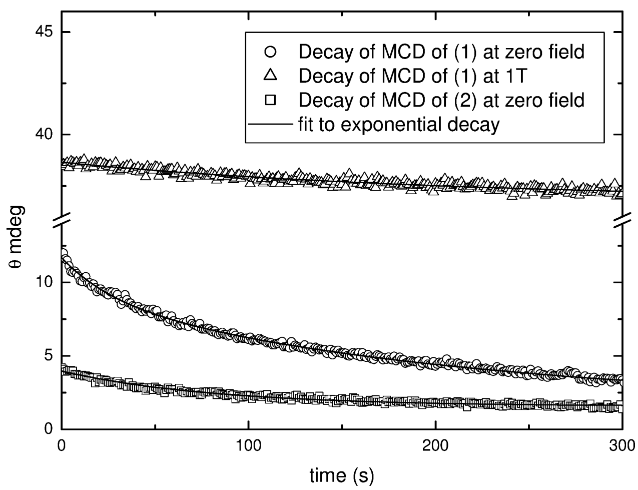

Fig. 5 Decay of the MCD at 445 nm of (**1**) and (**2**) after stepping the field from 5 T to zero field or from 2 T to 1 T.

The physical origin of the observed relaxation phenomena is unclear. However, further measurements eliminate certain possibilities. Relaxation of the magnetisation persists at 1.7 K with the beam shutter of the spectropolarimeter closed. The observed relaxation is therefore not caused by localised heating of the sample upon photon absorption. Dissolution of (**1**) into mixed organic solvent (70% v/v $CH_3CO_2CH_2CH_3$: 30% v/v $CHCl_3$) results in a glass at 1.7 K of poor transmittance but an MCD response is still observable for samples with effective concentration of approximately 10% of that in the polymer films. The decay of magnetisation at zero field is similar to that of the film samples (data not shown). It seems unlikely therefore that the magnetisation relaxation is caused by dipolar interactions between cages at the high effective concentrations (*ca.* 1 mM) of the film samples.

Conclusions

The Mn_6 cages (**1**)–(**3**) have MCD spectra which have bands at similar energies to the Mn(III) containing, mixed valence Mn_{12} series though the pattern of relative intensities is significantly different. The trinuclear precursor complex (4) has a distinct MCD spectrum, most notably lacking the positive band and shoulder at around 22 000 cm^{-1}. This may reflect the presence of the capping perchlorate ion, an extremely weak ligand. Weakening of the ligand field environment shifts the ^5E to $^3T_1$ transition higher in energy relative to the ^5E to $^5T_2$ transition in octahedral symmetry. The features at 22 000 cm^{-1} in (**1**) to (**3**) are therefore tentatively assigned to spin-forbidden transitions which are at higher energy in (**4**) and possibly masked by more intense charge transfer transitions.

Both (**1**) and (**2**) show MCD detected hysteresis in their response to an applied magnetic field at 1.7 K although they appear much softer magnets than Mn_{12} and equivalent samples in the solid state in which the hysteresis is detected by magnetic susceptibility. However, the absence of any such hysteresis in the 1.7 K MCD of (**3**) and (**4**) demonstrates that SMM behaviour persists for at least

Table 3 Fitted parameters for exponential decay of the MCD intensity of compounds (**1**) and (**2**). All timecourses were collected at zero field except * which was collected after stepping the field from 2 T to 1 T

Compound	Energy (× 10^3 cm^{-1})	y_0 (mdeg)	A_1 (mdeg)	t_1 (s)	A_2 (mdeg)	t_2 (s)
(**1**)	18.9	0.83	—	—	−1.7	202
(**1**)	22.5	1.61	2.67	27	7.4	206
(**1**)*	22.5	36.8	—	—	1.9	208
(**1**)	26.5	0.3	4.26	43	7.3	203
(**1**)	30.4	−0.25	−1.88	28	−3.53	169
(**2**)	22.3	1.56	2.4	82	—	—
(**2**)	26.5	0.38	2.7	74	—	—
(**2**)	30.1	−0.53	−1.1	58	—	—

some proportion of the ensemble of (**1**) and (**2**) upon casting into polymer film. The difference in behaviour from that in the solid state may be caused by relaxation of the structural distortions from which the ferromagnetic pairwise exchange originates on casting into PMMA film. Molecules in solid-state samples, be they powder or single crystal, are subject to crystal packing forces which are absent in the polymer matrix in which the samples were cast for MCD measurements. Whilst the MCD measurements show the hysteresis effects to persist for such isolated molecules it may be that relaxation of the structure lowers the average torsion angles within the clusters leading to weaker overall ferromagnetic exchange or possibly a change in spin ground state, an effective blocking temperature which is lower than the theoretical maximum and hence narrower hysteresis loops. This weakening of the ferromagnetic exchange may be such that even at 1.7 K one or more spin excited states are occupied due to overlap of spin manifolds. This distribution of net spin states could account for the observation of several relaxation rates of the magnetisation at 1.7 K. Alternatively, transverse components of the magnetic field may be inducing relaxation *via* a spin mixing mechanism.

Despite the narrowness of the observed hysteresis in (**1**) and (**2**), comparison of data to that acquired under identical conditions for (**3**) and (**4**) show the effects to be real. (**3**) and (**4**) have lower blocking temperatures on account of their smaller spin ground states and therefore have no hysteresis detectable by MCD at 1.7 K.

Comparison of the 4.2 K, 5 T MCD of (**1**)–(**4**) shows that the intensity of the band at approximately 26 500 cm^{-1} is diagnostic of the coordination environment (three six-coordinate *cf.* two six-coordinate and one five-coordinate) of the manganese ions. Since the change in coordination environment is induced by the same structural distortion which causes the change from dominant antiferromagnetic to ferromagnetic exchange within the $[Mn_3–\mu_3\text{-}0^{2-}]^{7+}$ moieties, the intensity of this feature is also diagnostic of the nature of the magnetic exchange within these triangular motifs. The presence of the capping perchlorate ion in (**4**) results in a weaker ligand field environment than in (**1**)–(**3**). This leads to significant changes in the 4.2 K, 5 T MCD, most notably the absence of the intense features at around 22 000 cm^{-1}. The feature at 26 000 cm^{-1} is unaffected by the change in ligand field, confirming that all Mn ions in (**4**) remain six-coordinate in the PMMA film. The hexanuclear cages are therefore readily distinguishable from their trinuclear precursors by the pattern of bands around 22 000 cm^{-1}.

Acknowledgements

We wish to thank EPSRC for grants GR/S57402/01, EP/H006737/1, EP/H011234/1, EP/H004106/1 and EP/E06471X/1. EKB also thanks The Leverhulme Trust.

References

1 D. Gatteschi and R. Sessoli, *Angew. Chem., Int. Ed.*, 2003, **42**, 268–297.
2 D., S. R. Gatteschi, J. Villain, *Molecular Nanomagnets*, Oxford University Press, 2006.
3 R. Sessoli, D. Gatteschi, A. Caneschi and M. A. Novak, *Nature*, 1993, **365**, 141–143.
4 R. Sessoli, H. L. Tsai, A. R. Schake, S. Y. Wang, J. B. Vincent, K. Folting, D. Gatteschi, G. Christou and D. N. Hendrickson, *J. Am. Chem. Soc.*, 1993, **115**, 1804–1816.
5 G. Aromí and E. K. Brechin, *Struct. Bonding*, 2006, **122**, 1–67.
6 H. Miyasaka, A. Saitoh and S. Abe, *Coord. Chem. Rev.*, 2007, **251**, 2622–2664.
7 G. Christou, *Polyhedron*, 2005, **24**, 2065–2075.
8 J. Cirera, E. Ruiz, S. Alvarez, F. Neese and J. Kortus, *Chem.–Eur. J.*, 2009, **15**, 4078–4087.
9 R. E. P. Winpenny, *J. Chem. Soc., Dalton Trans.*, 2002, 1–10.
10 J. T. Brockman, T. C. Stamatatos, W. Wernsdorfer, K. A. Abboud and G. Christou, *Inorg. Chem.*, 2007, **46**, 9160–9171.
11 S. Koizumi, M. Nihei, T. Shiga, M. Nakano, H. Nojiri, R. Bircherrl, O. Waldmann, S. T. Ochsenbein, H. U. Guedel, F. Fernandez-Alonso and H. Oshio, *Chem.–Eur. J.*, 2007, **13**, 8445–8453.
12 E. S. Koumousi, M. J. Manos, C. Lampropoulos, A. J. Tasiopoulos, W. Wernsdorfer, G. Christou and T. C. Stamatatos, *Inorg. Chem.*, 2010, **49**, 3077–3079.
13 D. C. Li, H. S. Wang, S. N. Wang, Y. P. Pan, C. J. Li, J. M. Dou and Y. Song, *Inorg. Chem.*, 2010, **49**, 3688–3690.
14 R. W. Saalfrank, A. Scheurer, R. Prakash, F. W. Heinemann, T. Nakajima, F. Hampel, R. Leppin, B. Pilawa, H. Rupp and P. Muller, *Inorg. Chem.*, 2007, **46**, 1586–1592.
15 S. J. Shah, C. M. Ramsey, K. J. Heroux, A. G. DiPasquale, N. S. Dalal, A. L. Rheingold, E. del Barco and D. N. Hendrickson, *Inorg. Chem.*, 2008, **47**, 9569–9582.
16 T. C. Stamatatos, V. Nastopoulos, A. J. Tasiopoulos, E. E. Moushi, W. Wernsdorfer, G. Christou and S. P. Perlepes, *Inorg. Chem.*, 2008, **47**, 10081–10089.
17 T. C. Stamatatos, G. Christou and Philosophical, *Philos. Trans. R. Soc. London, Ser. A*, 2008, **366**, 113–125.
18 T. C. Stamatatos and G. Christou, *Inorg. Chem.*, 2009, **48**, 3308–3322.
19 T. Taguchi, W. Wernsdorfer, K. A. Abboud and G. Christou, *Inorg. Chem.*, 2010, **49**, 199–208.
20 C. I. Yang, W. Wernsdorfer, G. H. Lee and H. L. Tsai, *J. Am. Chem. Soc.*, 2007, **129**, 456–457.
21 R. Inglis, L. F. Jones, C. J. Milios, S. Datta, A. Collins, S. Parsons, W. Wernsdorfer, S. Hill, S. P. Perlepes, S. Piligkos and E. K. Brechin, *Dalton Trans.*, 2009, 3403–3412.
22 L. F. Jones, M. E. Cochrane, B. D. Koivisto, D. A. Leigh, S. P. Perlepes, W. Wernsdorfer and E. K. Brechin, *Inorg. Chim. Acta*, 2008, **361**, 3420–3426.
23 L. F. Jones, C. J. Milios, A. Prescimone, M. Evangelisti and E. K. Brechin, *C. R. Chim.*, 2008, **11**, 1175–1181.
24 C. J. Milios, R. Inglis, L. F. Jones, A. Prescimone, S. Parsons, W. Wernsdorfer and E. K. Brechin, *Dalton Trans.*, 2009, 2812–2822.
25 C. J. Milios, S. Piligkos and E. K. Brechin, *Dalton Trans.*, 2008, 1809–1817.
26 C. J. Milios, A. Vinslava, W. Wernsdorfer, S. Moggach, S. Parsons, S. P. Perlepes, G. Christou and E. K. Brechin, *J. Am. Chem. Soc.*, 2007, **129**, 2754.
27 C. J. Milios, A. Vinslava, W. Wernsdorfer, A. Prescimone, P. A. Wood, S. Parsons, S. P. Perlepes, G. Christou and E. K. Brechin, *J. Am. Chem. Soc.*, 2007, **129**, 6547–6561.
28 S. M. J. Aubin, Z. M. Sun, H. J. Eppley, E. M. Rumberger, I. A. Guzei, K. Folting, P. K. Gantzel, A. L. Rheingold, G. Christou and D. N. Hendrickson, *Inorg. Chem.*, 2001, **40**, 2127–2146.
29 R. Inglis, S. M. Taylor, L. F. Jones, G. S. Papaefstathiou, S. P. Perlepes, S. Datta, S. Hill, W. Wernsdorfer and E. K. Brechin, *Dalton Trans.*, 2009, 9157–9168.
30 C. J. Milios, C. P. Raptopoulou, A. Terzis, F. Lloret, R. Vicente, S. P. Perlepes and A. Escuer, *Angew. Chem., Int. Ed.*, 2004, **43**, 210–212.
31 E. J. L. McInnes, E. Pidcock, V. S. Oganesyan, M. R. Cheesman, A. K. Powell and A. J. Thomson, *J. Am. Chem. Soc.*, 2002, **124**, 9219–9228.
32 D. Collison, M. Murrie, V. S. Oganesyan, S. Piligkos, N. R. J. Poolton, G. Rajaraman, G. M. Smith, A. J. Thomson, G. A. Timko, W. Wernsdorfer, R. E. P. Winpenny and E. J. L. McInnes, *Inorg. Chem.*, 2003, **42**, 5293–5303.
33 D. Collison, V. S. Oganesyan, S. Piligkos, A. J. Thomson, R. E. P. Winpenny and E. J. L. McInnes, *J. Am. Chem. Soc.*, 2003, **125**, 1168–1169.
34 D. M. Sherman and N. Vergo, *Am. Miner.*, 1988, **73**, 140–144.
35 A. Prescimone, C. J. Milios, S. Moggach, J. E. Warren, A. R. Lennie, J. Sanchez-Benitez, K. Kamenev, R. Bircher, M. Murrie, S. Parsons and E. K. Brechin, *Angew. Chem., Int. Ed.*, 2008, **47**, 2828–2831.
36 A. Prescimone, C. J. Milios, J. Sanchez-Benitez, K. V. Kamenev, C. Loose, J. Kortus, S. Moggach, M. Murrie, J. E. Warren, A. R. Lennie, S. Parsons and E. K. Brechin, *Dalton Trans.*, 2009, 4858–4867.

37 K. Awaga, Y. Suzuki, H. Hachisuka and K. Takeda, *J. Mater. Chem.*, 2006, **16**, 2516–2521.
38 P. Parois, S. A. Moggach, J. Sanchez-Benitez, K. V. Kamenev, A. R. Lennie, J. E. Warren, E. K. Brechin, S. Parsons and M. Murrie, *Chem. Commun.*, 2010, **46**, 1881–1883.
39 A. Sieber, R. Bircher, O. Waldmann, G. Carver, G. Chaboussant, H. Mutka and H. U. Gudel, *Angew. Chem., Int. Ed.*, 2005, **44**, 4239–4242.
40 O. Waldmann, G. Carver, C. Dobe, A. Sieber, H. U. Gudel and H. Mutka, *J. Am. Chem. Soc.*, 2007, **129**, 1526.
41 S. Bahr, C. J. Milios, L. F. Jones, E. K. Brechin, V. Mosser and W. Wernsdorfer, *New J. Chem.*, 2009, **33**, 1231–1236.
42 S. Carretta, T. Guidi, P. Santini, G. Amoretti, O. Pieper, B. Lake, J. van Slageren, F. El Hallak, W. Wernsdorfer, H. Mutka, M. Russina, C. J. Milios and E. K. Brechin, *Polyhedron*, 2009, **28**, 1940–1944.
43 J. R. Friedman, M. P. Sarachik, J. Tejada and R. Ziolo, *Phys. Rev. Lett.*, 1996, **76**, 3830–3833.
44 J. Villain, F. Hartmanboutron, R. Sessoli and A. Rettori, *Europhys. Lett.*, 1994, **27**, 159–164.
45 A. Wurger, *J. Phys.: Condens. Matter*, 1998, **10**, 10075–10099.